

Cite this: *J. Mater. Chem. C*, 2020, **8**, 15135

## A privileged ternary blend enabling non-fullerene organic photovoltaics with over 14% efficiency†

Jing Yan,<sup>‡a</sup> Yuan-Qiu-Qiang Yi,<sup>‡a</sup> Jianqi Zhang,<sup>‡b</sup> Huanran Feng,<sup>a</sup> Yanfeng Ma,<sup>a</sup> Xiangjian Wan,<sup>‡a</sup> Chenxi Li,<sup>a</sup> Zhixiang Wei<sup>‡b</sup> and Yongsheng Chen<sup>‡\*a</sup>

Two non-fullerene small molecule acceptors (NF-SMAs) **NT-4F** and **NT-4Cl** with halogenated end groups were designed and synthesized. When blended with **PM6**, the **NT-4Cl**-based binary device gave a power conversion efficiency (PCE) of 11.44% with a fill factor (FF) of 74.1% while the **NT-4F** binary system showed a PCE of 9.46%. To further broaden the absorption profile and fine-tune the morphology, **NCBDT-4Cl**, an acceptor with a similar chemical structure and identical molecular orientation to **NT-4Cl**, was selected as a combinatory component to the **PM6:NT-4Cl** system. As a result, the ternary device achieved a dramatically promoted PCE of 14.55% with a synergistically enhanced FF of 77.1% and a  $J_{sc}$  of 20.99 mA cm<sup>-2</sup> as well as a decreased energy loss ( $E_{loss}$ ) of 0.51 eV, which represents the best performance for NT-based NF-SMAs to date.

Received 11th June 2020,  
Accepted 7th July 2020

DOI: 10.1039/d0tc02778b

rsc.li/materials-c

### Introduction

Organic photovoltaics (OPVs) offer great opportunities to construct roll-to-roll printed flexible devices with light weight for future energy conversion.<sup>1–3</sup> Over the last five years, with tremendous successes and huge advantages of non-fullerene small molecule acceptors (NF-SMAs), OPVs have achieved great breakthroughs. Power conversion efficiencies (PCEs) of 16–18% can be achieved for both single junction and tandem cells owing to material design as well as device optimization.<sup>4–16</sup> Acceptor–donor–acceptor (A–D–A) architecture-based NF-SMAs provide a rich platform to manipulate and optimize the molecule design and film morphology and even the optoelectronic process.<sup>17,18</sup>

For the widely studied binary blend based OPVs, normally with a medium or narrow bandgap, the device performances are mainly limited by either comparatively low short-circuit current density ( $J_{sc}$ ) or low open-circuit voltage ( $V_{oc}$ ), and it is hard to obtain high values for both at the same time.<sup>19</sup> As such, to further elevate the PCEs of OPVs, achieving an excellent balance of both high  $J_{sc}$  and  $V_{oc}$  is a very promising approach to

tackle the abovementioned issues.<sup>20,21</sup> Thus, using two or even more components in the photoactive layer to obtain a wide and complementary light absorption spectrum and form a privileged blend film morphology is an ideal method to improve the photovoltaic performances in OPVs, along with highly balanced  $J_{sc}$  and  $V_{oc}$ <sup>22</sup> and potentially enhanced fill factor (FF).<sup>23–27</sup> Besides, note that the ternary OPV performances strongly depend on the match of different photoactive materials to form a suitable band structure and ideal film morphology,<sup>28</sup> which may simultaneously reduce the energy loss<sup>29</sup> and achieve efficient charge generation and transport properties.<sup>30,31</sup> To overcome the drawbacks of traditional fullerenes and their derivatives, which have difficulty in modifying the band structure and absorption spectrum, the use of one polymer donor and two NF-SMAs as photoactive blends to construct high-performance ternary OPVs is a popular and ideal strategy to achieve a wide absorption range and obtain suitable energy level alignment.<sup>32</sup> In addition, the energy losses of the NF-SMA based OPVs can be efficiently suppressed owing to the need for only a small driving force for the charge separation process.<sup>29,33–36</sup> To this end, there are some successful ternary systems with only NF-SMAs as acceptors to achieve high device performances and low energy losses.<sup>37–43</sup> Notably, these NF-SMAs normally have high halogenation contents on their end-groups to form a suitable morphology, achieve high mobilities and thus obtain a high FF. As such, the privileged ternary blend including one polymer donor and two NF-SMAs could elevate the device performance to an expected high level with ideal morphology. Furthermore, constructing and studying such a highly efficient ternary device can help in deeply understanding the working mechanism

<sup>a</sup> State Key Laboratory and Institute of Elemento-Organic Chemistry, The Centre of Nanoscale Science and Technology and Key Laboratory of Functional Polymer Materials, Renewable Energy Conversion and Storage Center (RECAST), College of Chemistry, Nankai University, Tianjin, 300071, China.  
E-mail: yschen99@nankai.edu.cn

<sup>b</sup> Key Laboratory of Nanosystem and Hierarchical Fabrication, National Center for Nanoscience and Technology, Beijing 100190, P. R. China

† Electronic supplementary information (ESI) available. See DOI: 10.1039/d0tc02778b

‡ These authors have contributed equally to this work.

and provide guidelines for future applications in the OPV community.

Previously, we have reported a NF-SMA named NTIC using NT (hexacyclic naphthalene(cyclopentadithiophene)) as the central core unit and INCN (2-(3-oxo-2,3-dihydro-1*H*-inden-1-ylidene)malononitrile) as the end group. When blended with PBDB-T as the donor, the binary device gave a PCE of 8.63% with a limited  $J_{sc}$  and FF.<sup>44</sup> In consideration of the superiority of halogenation onto NF-SMAs with red-shifted absorption, facilitated crystallinity and charge mobility, to obtain higher  $J_{sc}$  and FF,<sup>22,45–50</sup> in this study, we have designed and synthesized two NF-SMAs with an identical conjugated core of NT and halogenated INCN as end groups, namely, NT-4F and NT-4Cl. Paired with polymer donor PM6, the NT-4F-based device gave a PCE of 9.46% while the NT-4Cl-based device exhibited a PCE of 11.44% with a  $J_{sc}$  of 16.62 mA cm<sup>-2</sup>, an FF of 74.1% and a  $V_{oc}$  of 0.929 V. Furthermore, a combinatory acceptor NCBDT-4Cl<sup>51</sup> was incorporated into the NT-4Cl-based host system due to its similar chemical structure and effective absorption in the near-infrared region. The optimal ternary OPV device achieved a significantly enhanced PCE of 14.55% with a simultaneously much increased  $J_{sc}$  of 20.99 mA cm<sup>-2</sup> and an FF of 77.1%, a  $V_{oc}$  of 0.899 V and a lowered  $E_{loss}$  of 0.51 eV, which is the best performance for NT-based photovoltaic materials to date.

## Results and discussion

### Synthesis and characterization

The target molecules NT-4F and NT-4Cl were synthesized through Knoevenagel condensation between the dialdehyde intermediate and fluorinated and chlorinated ending groups, respectively. The detailed synthesis procedures and characterization including nuclear magnetic resonance (NMR) and mass spectra are presented in the ESI.† Both the molecules exhibited good solubility

in common organic solvents such as chloroform, dichloromethane and chlorobenzene.

The ultraviolet-visible (UV-vis) absorption spectra of NT-4Cl and NT-4F are shown in Fig. 1b. In dilute chloroform solutions, NT-4Cl and NT-4F share similar absorption profiles with maximum absorption peaks at 672 and 661 nm, respectively. In solid film states, NT-4Cl and NT-4F display absorption peaks located at 706 nm and 681 nm, which were red-shifted by 34 and 22 nm, respectively. A more bathochromic absorption for NT-4Cl indicates a more ordered and closer  $\pi$ - $\pi$  intermolecular stacking, which is in favor of a promoted  $J_{sc}$  and FF. The optical bandgaps ( $E_g^{opt}$ ) of NT-4Cl and NT-4F estimated from thin-film absorption onsets are 1.64 and 1.68 eV, respectively.

The frontier molecular orbital energy levels of NT-4Cl and NT-4F were measured by electrochemical cyclic voltammetry (CV) referenced to the energy level of Fc/Fc<sup>+</sup> (-4.8 eV below the vacuum level) (Fig. S2 in the ESI†). In comparison to NT-4F, NT-4Cl shows a slightly deeper lowest unoccupied molecular orbital (LUMO) level (-3.92 eV vs. -3.86 eV) and a similar highest occupied molecular orbital (HOMO) level (-5.89 eV vs. -5.88 eV) (Table 1).

### Photovoltaic properties

In order to evaluate the photovoltaic performances of NT-4Cl and NT-4F, solution-processed OPV cells were fabricated with a

Table 1 Optical and electrochemical parameters of NT-4Cl, NT-4F and NCBDT-4Cl

Comp.	$\lambda_{max}^{sol}$ (nm)	$\lambda_{max}^{film}$ (nm)	$\lambda_{edge}^{film}$ (nm)	$E_g^{opt}$ (eV)	HOMO (eV)	LUMO (eV)	$E_g^{CV}$ (eV)
NT-4F	661	683	738	1.68	-5.88	-3.86	2.02
NT-4Cl	672	706	755	1.64	-5.89	-3.92	1.97
NCBDT-4Cl	749	798	885	1.40	-5.60	-4.02	1.58

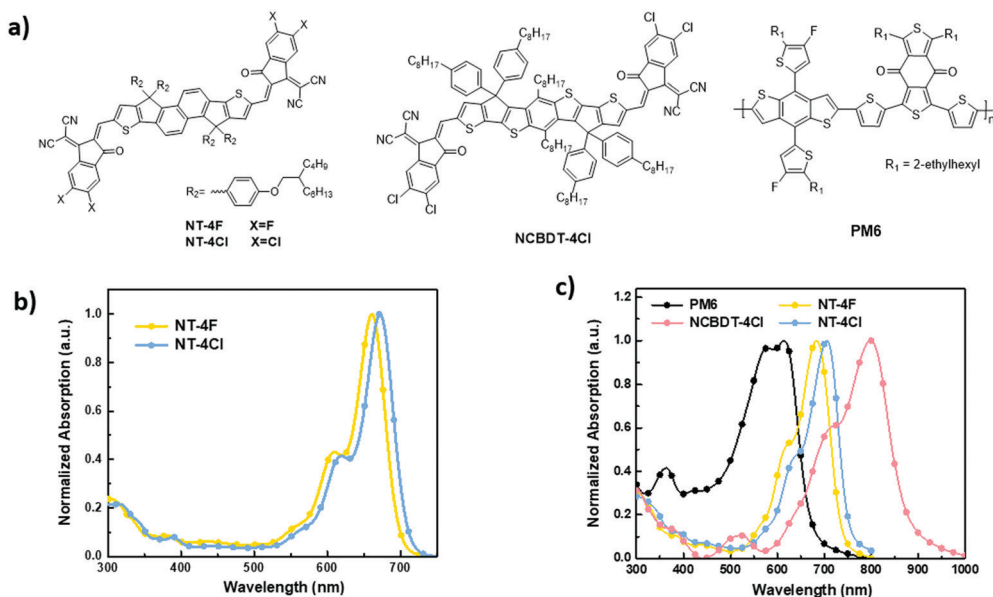


Fig. 1 (a) Chemical structures of NT-4F, NT-4Cl, NCBDT-4Cl and PM6; UV-vis absorption spectra of (b) the acceptors in chloroform solutions and (c) the donors and acceptors in films.

conventional structure of ITO/PEDOT:PSS/PM6:acceptors/PDINO/Al (Fig. 2a), where PEDOT:PSS and PDINO represent poly(3,4-ethylene-dioxythiophene):poly(styrenesulfonate) and perylene diimide functionalized with amino *N*-oxide, respectively. The wide-bandgap polymer PM6 was employed as the donor due to its matched energy level and complementary absorption (Fig. 1c and 2b). Through systematic device optimization (Table S1, ESI<sup>†</sup>), chlorobenzene and 1,8-diiodooctane (0.5% volume) were selected as the processing solvent and solvent additive, respectively, and the optimal D/A ratio was 1 : 1.2 for both blends. As a result, the PM6:NT-4F based device achieved a PCE of 9.46% with a  $J_{sc}$  of 13.87 mA cm<sup>-2</sup>, a  $V_{oc}$  of 0.958 V, an FF of 71.2% and an energy loss ( $E_{loss}$ , defined as  $E_{loss} = E_g^{opt} - eV_{oc}$ , where  $E_g^{opt}$  refers to the optical bandgap of the acceptor) of 0.72 eV. However, the OPV device based on PM6:NT-4Cl gave a promoted PCE of 11.44% with a  $J_{sc}$  of 16.62 mA cm<sup>-2</sup>, a  $V_{oc}$  of 0.929 V, an FF of 74.1% and an  $E_{loss}$  of 0.71 eV (Table 2). Benefiting from the redshift absorption of NT-4Cl, a higher  $J_{sc}$  can be achieved for the PM6:NT-4Cl blend. Also, a higher FF implies that chlorination helped in forming ideal phase separation with more efficient charge transfer as discussed below.

The external quantum efficiency (EQE) spectra of the two devices are shown in Fig. 2d. Compared with the relatively lower and slightly narrower photoresponse from 300 to 750 nm of the PM6:NT-4F-based device, the PM6:NT-4Cl-based device achieves a stronger and broader photoresponse from 300 to ~800 nm, implying a more efficient charge transfer between PM6 and NT-4Cl. The integrated photocurrents of PM6:NT-4F and PM6:NT-4Cl calculated from the EQE spectra are 13.97 and 16.40 mA cm<sup>-2</sup>, respectively, which are well consistent with the  $J_{sc}$  values obtained from the corresponding  $J$ - $V$  curves within 5% mismatch. For the binary PM6:NT-4Cl system, the moderate  $J_{sc}$  limited by the absorption onset of the blend film hindered the overall photovoltaic performance. In order to pursue a higher PCE with an elevated  $J_{sc}$  value by broadening the absorption range, together with maintaining  $V_{oc}$  and potentially enhanced FF, a third component NCBDT-4Cl with a similar chemical structure to NT-4Cl was introduced to fabricate ternary devices. The introduction of NCBDT-4Cl further extended the light absorption range to 880 nm and formed complementary absorption with the host binary materials, which helped the ternary blend to utilize photons from the visible light to the

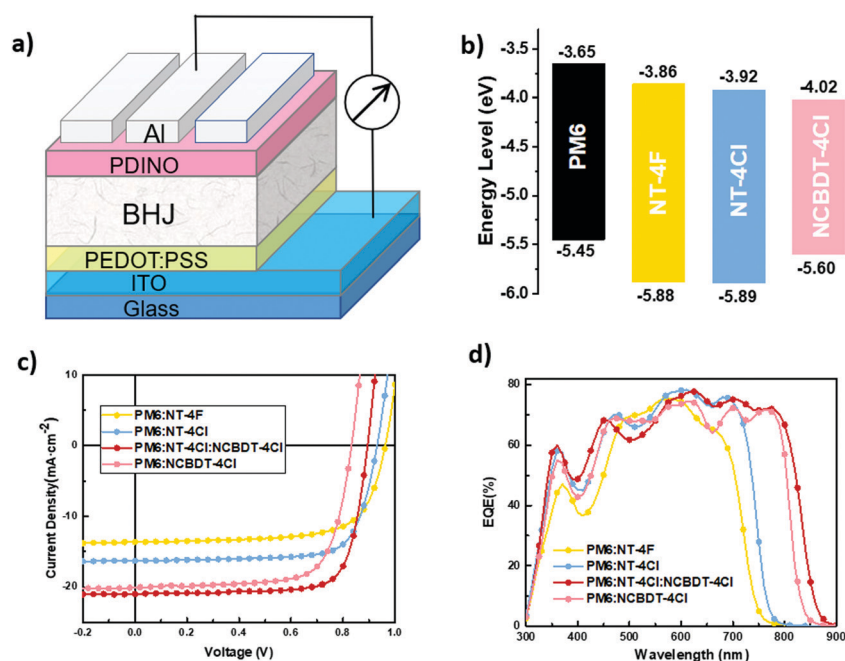


Fig. 2 (a) Diagram of the conventional device structure; (b) energy level diagram of the donor and acceptors; (c) current density–voltage ( $J$ - $V$ ) curves and (d) EQE spectra of binary and ternary OPV cells.

Table 2 Optimal device parameters of the binary and ternary devices under an AM 1.5G illumination (100 mW cm<sup>-2</sup>)

Active layers <sup>a</sup>	$V_{oc}$ (V)	$J_{sc}$ (mA cm <sup>-2</sup> )	$J_{sc}^{cal}$ (mA cm <sup>-2</sup> )	FF (%)	PCE <sup>b</sup> (%)	$E_{loss}$ (eV)
PM6:NT-4F (1:1.2)	0.958	13.87	13.97	71.2	9.46 (9.14)	0.72
PM6:NT-4Cl (1:1.2)	0.929	16.62	16.40	74.1	11.44 (11.40)	0.71
PM6:NT-4Cl:NCBDT-4Cl (1:0.6:0.4)	0.899	20.99	20.43	77.1	14.55 (14.27)	0.51
PM6:NCBDT-4Cl (1:1)	0.833	20.07	19.95	72.0	12.04 (12.00)	0.57

<sup>a</sup> The weight ratios of each component. <sup>b</sup> The average values with standard deviations obtained from 20 devices.

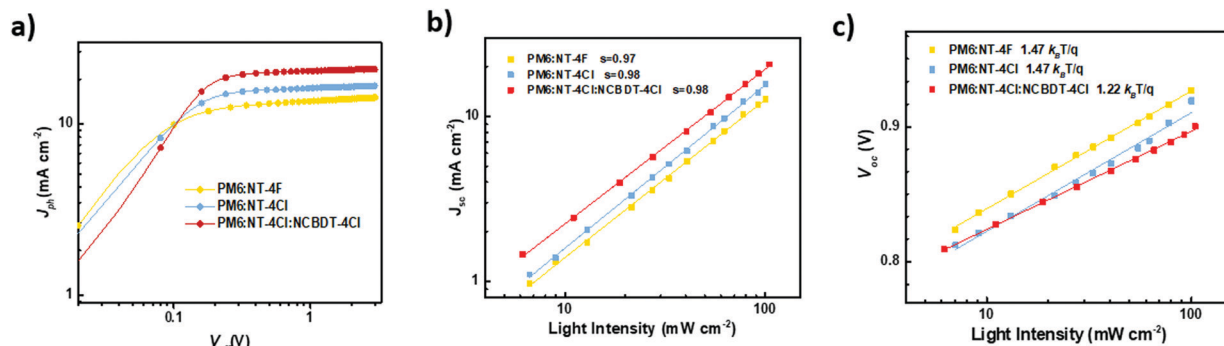


Fig. 3 (a)  $J_{ph}$  versus  $V_{eff}$ ; (b) light-intensity dependence of  $J_{sc}$ ; (c) light-intensity dependence of  $V_{oc}$  in the optimized binary and ternary devices.

near-infrared region. Meanwhile, a similar chemical backbone of chlorinated INCN may help in tuning the morphology and facilitating the molecular crystallinity. The ternary device was optimized by adjusting the **PM6:NT-4Cl:NCBDT-4Cl** ratios. As a result, when 40 wt% **NCBDT-4Cl** was added, the ternary blend yielded a significantly enhanced PCE of 14.55% with synergistically improved  $J_{sc}$  of 20.99 mA cm<sup>-2</sup>, a remarkable FF of 77.1% and a satisfactory  $V_{oc}$  of 0.899 V, which is the highest PCE value for NT-based NF-SMAs at present. As displayed in the EQE spectra, the ternary system featured a broadened EQE response covering 300–880 nm, with 80% photoresponse in the range of 550–700 nm, implying the efficient photon harvesting and charge collection process in ternary OPVs. The impressive FF may be ascribed to the more organized molecular packing and more efficient charge separation and collection.<sup>52</sup> In addition, the  $E_{loss}$  was measured to be merely 0.51 eV, indicating that the construction of the ternary system is a practical method to reduce the energy loss.

Investigations into exciton dissociation and the charge collection process were conducted using the photocurrent density ( $J_{ph}$ ) versus the effective voltage ( $V_{eff}$ ).<sup>53</sup> As shown in Fig. 3a, when  $V_{eff}$  exceeds 1.6 V, the  $J_{ph}$  values for both binary and ternary devices reach saturation ( $J_{sat}$ ), suggesting that charge recombination is minimized at higher voltage due to the high internal electric field in the devices. Furthermore, the exciton dissociation efficiency ( $\eta_{diss}$ ) and charge collection efficiency ( $\eta_{coll}$ ) can be estimated by calculating the ratios of  $J_{ph}^*/J_{sat}$  and  $J_{ph}^\# / J_{sat}$ , where  $J_{ph}^*$  and  $J_{ph}^\#$  represent the  $J_{ph}$  under short circuit and maximal power output conditions, respectively.<sup>54,55</sup> Compared with 95.18% for the **NT-4F** based device, the  $J_{ph}^*/J_{sat}$  ratios for the **NT-4Cl**-based binary and ternary devices were 96.86% and 97.70%, respectively. On the other hand, the  $J_{ph}^\# / J_{sat}$  ratios for the **PM6:NT-4F**, **PM6:NT-4Cl** and **PM6:NT-4Cl:NCBDT-4Cl** blends were 83.41%, 86.13% and 87.31%, respectively. The higher  $\eta_{diss}$  and  $\eta_{coll}$  values for the **NT-4Cl**-based system represent more efficient charge extraction and transport, thus leading to higher FFs.

Bimolecular charge recombination behaviors were determined using the correlations between light intensity ( $P$ ) and  $J_{sc}$ . The relationship between  $J_{sc}$  and  $P$  can be described as  $J_{sc} \propto P^\alpha$ , where the exponent  $\alpha$  refers to the extent of bimolecular recombination. When  $\alpha = 1$ , the devices can be modelled as an ideal diode with negligible bimolecular recombination, and an  $\alpha$  value smaller than 1 indicates that bimolecular recombination may be existing in

the blends.<sup>56,57</sup> As depicted in Fig. 3b, the exponent  $\alpha$  values for devices based on **PM6:NT-4F**, **PM6:NT-4Cl** and **PM6:NT-4Cl:NCBDT-4Cl** were 0.97, 0.98 and 0.98, respectively, implying highly suppressed bimolecular recombination in **NT-4Cl**-based devices. The light-intensity dependence of  $V_{oc}$  was also tested to study the trap-assisted recombination properties in the blends. A slope at  $2k_B T/q$  implies that the trap-assisted recombination mechanism prevails in the working device, where  $k_B$  is Boltzmann's constant,  $T$  is the temperature, and  $q$  is the elementary charge. Otherwise, a slope at  $k_B T/q$  reflects the dominant bimolecular recombination.<sup>58</sup> As displayed in Fig. 3c, the slopes for devices based on **PM6:NT-4F**, **PM6:NT-4Cl** and **PM6:NT-4Cl:NCBDT-4Cl** were 1.47, 1.47 and 1.22  $k_B T/q$ , respectively. These results indicate that there was weak trap-assisted recombination in **NT-4Cl**-based ternary devices.

The charge mobilities of both binary and ternary active layers were measured by the space-charge-limited current (SCLC) method using the electron-only and hole-only devices, respectively.<sup>59</sup> The calculated electron ( $\mu_e$ ) and hole mobilities ( $\mu_h$ ) for **NT-4F**- and **NT-4Cl**-based binary devices were  $3.29 \times 10^{-4}/1.05 \times 10^{-4}$  and  $7.84 \times 10^{-4}/4.61 \times 10^{-4}$  cm<sup>2</sup> V<sup>-1</sup> s<sup>-1</sup>, with corresponding  $\mu_e/\mu_h$  ratios of 3.13 and 1.70, respectively. These results demonstrate that chlorination to NT-based NF-SMAs proves to be a feasible manner to obtain higher and more balanced charge mobilities. After the introduction of **NCBDT-4Cl**, the ternary blend yielded electron and hole mobilities of  $7.65 \times 10^{-4}/6.51 \times 10^{-4}$  cm<sup>2</sup> V<sup>-1</sup> s<sup>-1</sup>, with  $\mu_e/\mu_h$  of 1.18. The relatively low  $\mu_e$  and  $\mu_h$  of **NCBDT-4Cl**-based binary systems ( $1.99 \times 10^{-4}/3.94 \times 10^{-4}$  cm<sup>2</sup> V<sup>-1</sup> s<sup>-1</sup>, with  $\mu_e/\mu_h$  of 0.51) suggested that the improved and more balanced charge mobilities for the ternary device can be ascribed to the optimization of the morphology as discussed below. The enhanced charge transport properties made contributions to the suppressed charge accumulation and recombination, thus leading to the simultaneously promoted  $J_{sc}$  and FF in the ternary system.

### Morphology characterization

The morphology of the active layers was characterized by atomic force microscopy (AFM) and transmission electron microscopy (TEM). From AFM images in Fig. S7a–c (ESI<sup>+</sup>), compared with the **PM6:NT-4F** blend film with a relatively large root-mean-square roughness (RMS) of 2.64 nm, the **NT-4Cl**-based binary and ternary films possessed a decreased RMS of 2.08 and 2.20 nm, respectively,

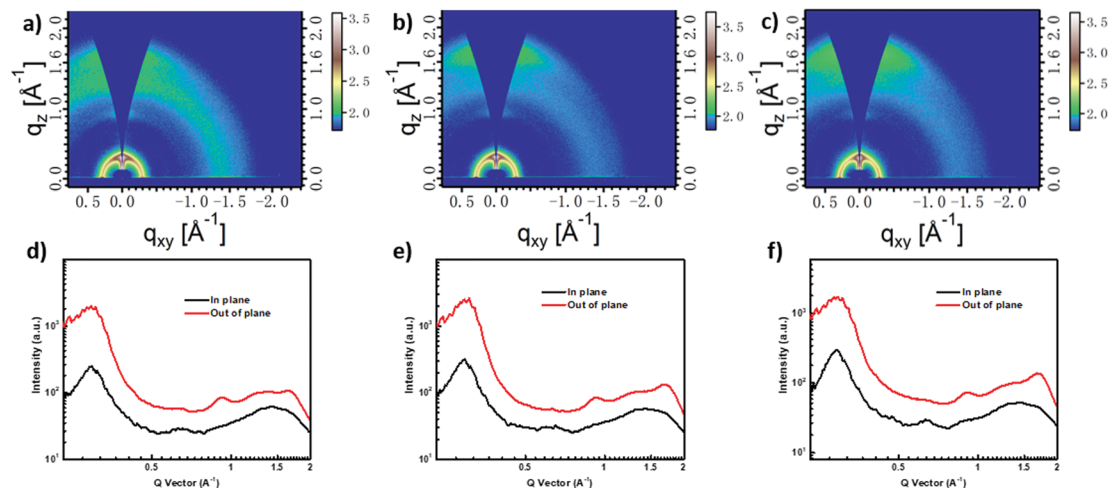


Fig. 4 GIWAXS patterns and in-plane and out-of-plane line cuts of the corresponding GIWAXS patterns for (a and d) **PM6:NT-4F**, (b and e) **PM6:NT-4Cl**, and (c and f) **PM6:NT-4Cl:NCBDT-4Cl** blend films.

with more uniform and smooth surfaces. As displayed in TEM images (Fig. S7d–f, ESI†), the **PM6:NT-4Cl:NCBDT-4Cl** film showed a more obvious phase separation. The outstanding nanoscale morphologies were beneficial for exciton dissociation and charge transport in support of high FFs.<sup>60–62</sup>

To further understand the film morphologies at nanoscale, grazing incidence wide-angle X-ray scattering (GIWAXS) testing was employed to investigate the intermolecular packing behaviors of the active layers. As depicted in Fig. 4a–c for the GIWAXS patterns and Fig. 4d–f for the corresponding line-cuts, all these three blends exhibited a preferred face-on orientation with lamellar diffraction peaks (100) in the in-plane (IP) direction and  $\pi$ - $\pi$  stacking peaks (010) in the out-of-plane (OOP) direction.<sup>63</sup> The corresponding parameters are summarized in Table 3. For the binary blends, the GIWAXS diffractions were mainly dominated by the polymer diffraction signals. Their (100) and (010) diffraction peaks for **PM6:NT-4F** and **PM6:NT-4Cl** were located at  $q_{xy} = 0.296/0.295 \text{ \AA}^{-1}$  and  $q_z = 1.66/1.68 \text{ \AA}^{-1}$ , with the corresponding alkyl-to-alkyl distance ( $d_l$ ) of 21.23/21.29 Å and a  $\pi$ - $\pi$  stacking distance ( $d_\pi$ ) of 3.79/3.74 Å, respectively. In spite of similar peak locations, the **PM6:NT-4Cl** blend showed a more pronounced (010) peak with stronger intensity, indicative of a more ordered  $\pi$ - $\pi$  stacking mode. As for the ternary blend, (100) and (010) diffraction peaks appeared at 0.290 and 1.69  $\text{\AA}^{-1}$ , with corresponding  $d_l$  and  $d_\pi$  of 21.30 and 3.72 Å, respectively.

Furthermore,  $\pi$ - $\pi$  stacking coherence length (CCL, estimated from the Scherrer's equation  $CCL = 2\pi k/\text{FWHM}$ , where FWHM refers to the full-width at half-maximum of the (010) peak along the  $q_z$  axis for the face-on crystallite) was adopted to evaluate the distance over which the crystalline order is preserved.<sup>64</sup> As a result, an enlarged CCL value of 23.70 Å for the ternary system demonstrated a more organized molecular packing feature, which was in favor of excellent charge transport characteristics.<sup>65</sup> The defined micromorphology and intermolecular packing in the ternary blend imply that **NCBDT-4Cl** possesses satisfactory miscibility with the primary acceptor **NT-4Cl**, which may be ascribed to their similar chemical backbones and the identical molecular orientation.<sup>37</sup>

## Conclusions

In summary, we have designed and synthesized two NF-SMAs, **NT-4F** and **NT-4Cl**, with halogenated end groups. Compared to the **PM6:NT-4F** based device with a PCE of 9.46%, the **PM6:NT-4Cl** based device gave a higher PCE of 11.44%. Upon introduction of a third component **NCBDT-4Cl** with a similar chemical structure to **NT-4Cl**, the ternary device yielded a dramatically enhanced PCE of 14.55% with a remarkable FF of over 77%. These results demonstrate that the fabrication of ternary OPVs is a feasible solution to achieve synergistically promoted  $J_{sc}$ , FF and balanced  $V_{oc}$  with privileged morphology.

## Conflicts of interest

There are no conflicts to declare.

## Acknowledgements

The authors gratefully acknowledge the financial support from MOST (2019YFA0705900, 2016YFA0200200) and NSFC (21935007, 51873089, 51773095) of China, Tianjin City (17JCQJC44500) and the 111 Project (B12015).

Table 3 The summarized parameters for the blend films obtained from GIWAXS

Active layers	Lamellar (100)	$\pi$ - $\pi$ stacking (010)		
	$d_l^a$ [Å] [ $q_{xy}$ ( $\text{\AA}^{-1}$ )]	$d_\pi^b$ [Å] [ $q_z$ ( $\text{\AA}^{-1}$ )]	FWHM ( $\text{\AA}^{-1}$ )	CCL (Å)
<b>PM6:NT-4F</b>	21.23 (0.296)	3.79 (1.66)	0.262	21.34
<b>PM6:NT-4Cl</b>	21.29 (0.295)	3.74 (1.68)	0.256	21.84
<b>PM6:NT-4Cl:NCBDT-4Cl</b>	21.30 (0.290)	3.72 (1.69)	0.236	23.70

<sup>a</sup> (100) diffraction peak along the  $q_{xy}$  axis. <sup>b</sup> (010) diffraction peak along the  $q_z$  axis.

## Notes and references

- G. Yu, J. Gao, J. C. Hummelen, F. Wudl and A. J. Heeger, *Science*, 1995, **270**, 1789.
- G. Li, R. Zhu and Y. Yang, *Nat. Photonics*, 2012, **6**, 153.
- Y. W. Li, G. Y. Xu, C. H. Cui and Y. Li, *Adv. Energy Mater.*, 2018, **8**, 28.
- X. Xu, K. Feng, Y. W. Lee, H. Y. Woo, G. Zhang and Q. Peng, *Adv. Funct. Mater.*, 2020, **30**, 1907570.
- Z. Zhou, W. Liu, G. Zhou, M. Zhang, D. Qian, J. Zhang, S. Chen, S. Xu, C. Yang, F. Gao, H. Zhu, F. Liu and X. Zhu, *Adv. Mater.*, 2020, **32**, 8.
- K. Jiang, Q. Wei, J. Lai, Z. Peng, H. Kim, J. Yuan, L. Ye, H. Ade, Y. Zou and H. Yan, *Joule*, 2019, **3**, 3020.
- Y. Cui, H. Yao, J. Zhang, T. Zhang, Y. Wang, L. Hong, K. Xian, B. Xu, S. Zhang, J. Peng, Z. Wei, F. Gao and J. Hou, *Nat. Commun.*, 2019, **10**, 2515.
- L. Meng, Y. Zhang, X. Wan, C. Li, X. Zhang, Y. Wang, X. Ke, Z. Xiao, L. Ding, R. Xia, H. Yip, Y. Cao and Y. Chen, *Science*, 2018, **361**, 1094.
- Y. Lin, Y. Firdaus, M. I. Nugraha, F. Liu, S. Karuthedath, A. H. Emwas, W. M. Zhang, A. Seitkhan, M. Neophytou, H. Faber, E. Yengel, I. McCulloch, L. Tsetseris, F. Laquai and T. D. Anthopoulos, *Adv. Sci.*, 2020, **7**, 9.
- L. Zhan, S. Li, T. Lau, Y. Cui, X. Lu, M. Shi, C. Li, H. Li, J. Hou and H. Chen, *Energy Environ. Sci.*, 2020, **13**, 635.
- L. Liu, Y. Kan, K. Gao, J. Wang, M. Zhao, H. Chen, C. Zhao, T. Jiu, A. K. Jen and Y. Li, *Adv. Mater.*, 2020, **32**, 7.
- Y. Lin, B. Adilbekova, Y. Firdaus, E. Yengel, H. Faber, M. Sajjad, X. Zheng, E. Yarali, A. Seitkhan, O. M. Bakr, A. El-Labban, U. Schwingenschlögl, V. Tung, I. McCulloch, F. Laquai and T. D. Anthopoulos, *Adv. Mater.*, 2019, **31**, 1902965.
- F. Huang, *Acta Polym. Sin.*, 2018, **9**, 1141–1143.
- Q. Liu, Y. Jiang, K. Jin, J. Qin, J. Xu, W. Li, J. Xiong, J. Liu, Z. Xiao, K. Sun, S. Yang, X. Zhang and L. Ding, *Sci. Bull.*, 2020, **65**, 272.
- Z. Luo, R. Sun, C. Zhong, T. Liu, G. Zhang, Y. Zou, X. Jiao, J. Min and C. Yang, *Sci. China: Chem.*, 2020, **63**, 361.
- Q. An, J. Wang, W. Gao, X. Ma, Z. Hu, J. Gao, C. Xu, M. Hao, X. Zhang, C. Yang and F. Zhang, *Sci. Bull.*, 2020, **65**, 538.
- X. Wan, C. Li, M. Zhang and Y. Chen, *Chem. Soc. Rev.*, 2020, **49**, 2828.
- M. Li, Y. Liu, W. Ni, F. Liu, H. Feng, Y. Zhang, T. Liu, H. Zhang, X. Wan, B. Kan, Q. Zhang, T. P. Russell and Y. Chen, *J. Mater. Chem. A*, 2016, **4**, 10409.
- M. Gratzel, *Philos. Trans. R. Soc., A*, 2007, **365**, 993.
- B. Minnaert and M. Burgelman, *Prog. Photovoltaics*, 2007, **15**, 741.
- J. Hou, O. Inganäs, R. H. Friend and F. Gao, *Nat. Mater.*, 2018, **17**, 119.
- H. Zhang, H. Yao, J. Hou, J. Zhu, J. Zhang, W. Li, R. Yu, B. Gao, S. Zhang and J. Hou, *Adv. Mater.*, 2018, **30**, 7.
- L. Lu, M. A. Kelly, W. You and L. Yu, *Nat. Photonics*, 2015, **9**, 491.
- H. Li, K. Lu and Z. Wei, *Adv. Energy Mater.*, 2017, **7**, 20.
- N. Gasparini, A. Salleo, I. McCulloch and D. Baran, *Nat. Rev. Mater.*, 2019, **4**, 229.
- T. Liu, Z. Luo, Y. Chen, T. Yang, Y. Xiao, G. Zhang, R. Ma, X. Lu, C. Zhan, M. Zhang, C. Yang, Y. Li, J. Yao and H. Yan, *Energy Environ. Sci.*, 2019, **12**, 2529.
- R. Yu, H. Yao and J. Hou, *Adv. Energy Mater.*, 2018, **8**, 9.
- W. Huang, P. Cheng, Y. Yang, G. Li and Y. Yang, *Adv. Mater.*, 2018, **30**, 24.
- Y. Ji, L. Xu, X. Hao and K. Gao, *Sol. RRL*, 2020, **4**, 2000130.
- T. Ameri, P. Khoram, J. Min and C. J. Brabec, *Adv. Mater.*, 2013, **25**, 4245.
- L. Yang, L. Yan and W. You, *J. Phys. Chem. Lett.*, 2013, **4**, 1802.
- W. D. Xu and F. Gao, *Mater. Horiz.*, 2018, **5**, 206.
- J. Yao, T. Kirchartz, M. S. Vezie, M. A. Faist, W. Gong, Z. He, H. Wu, J. Troughton, T. Watson, D. Bryant and J. Nelson, *Phys. Rev. Appl.*, 2015, **4**, 10.
- J. Zhang, L. Zhu and Z. Wei, *Small Methods*, 2017, **1**, 1700258.
- S. Li, L. Zhan, C. Sun, H. Zhu, G. Zhou, W. Yang, M. Shi, C. Li, J. Hou, Y. Li and H. Chen, *J. Am. Chem. Soc.*, 2019, **141**, 3073.
- J. Liu, S. Chen, D. Qian, B. Gautam, G. Yang, J. Zhao, J. Bergqvist, F. Zhang, W. Ma, H. Ade, O. Inganäs, K. Gundogdu, F. Gao and H. Yan, *Nat. Energy*, 2016, **1**, 16089.
- B. Kan, Y.-Q.-Q. Yi, X. Wan, H. Feng, X. Ke, Y. Wang, C. Li and Y. Chen, *Adv. Energy Mater.*, 2018, **8**, 1800424.
- X. Du, Y. Yuan, L. Zhou, H. Lin, C. Zheng, J. Luo, Z. Chen, S. Tao and L. Liao, *Adv. Funct. Mater.*, 2020, **30**, 13.
- X. Ma, Q. An, O. A. Ibraikulov, P. Leveque, T. Heiser, N. Leclerc, X. Zhang and F. Zhang, *J. Mater. Chem. A*, 2020, **8**, 1265.
- H. Wang, Z. Zhang, J. Yu, P. Lin, C. Chueh, X. Liu, S. Guang, S. Qu and W. Tang, *ACS Appl. Mater. Interfaces*, 2020, **12**, 21633.
- C. Wang, W. Zhang, X. Meng, J. Bergqvist, X. Liu, Z. Genene, X. Xu, A. Yartsev, O. Inganäs, W. Ma, E. Wang and M. Fahlman, *Adv. Energy Mater.*, 2017, **7**, 1700390.
- R. Yu, H. Yao, Y. Cui, L. Hong, C. He and J. Hou, *Adv. Mater.*, 2019, **31**, 8.
- P. Cheng, M. Zhang, T. Lau, Y. Wu, B. Jia, J. Wang, C. Yan, M. Qin, X. Lu and X. Zhan, *Adv. Mater.*, 2017, **29**, 7.
- Y.-Q.-Q. Yi, H. Feng, M. Chang, H. Zhang, X. Wan, C. Li and Y. Chen, *J. Mater. Chem. A*, 2017, **5**, 17204.
- G. P. Kini, S. J. Jeon and D. K. Moon, *Adv. Mater.*, 2020, **32**, 38.
- Y. Wang, Y. Zhang, N. Qiu, H. Feng, H. Gao, B. Kan, Y. Ma, C. Li, X. Wan and Y. Chen, *Adv. Energy Mater.*, 2018, **8**, 7.
- S. Sun, Y. Huo, M. Li, X. Hu, H. Zhang, Y. Zhang, Y. Zhang, X. Chen, Z. Shi, X. Gong, Y. Chen and H. Zhang, *ACS Appl. Mater. Interfaces*, 2015, **7**, 19914.
- Y. Chen, T. Liu, H. Hu, T. Ma, J. Lai, J. Zhang, H. Ade and H. Yan, *Adv. Energy Mater.*, 2018, **8**, 8.
- H. Feng, Y.-Q.-Q. Yi, X. Ke, J. Yan, Y. Zhang, X. Wan, C. Li, N. Zheng, Z. Xie and Y. Chen, *Adv. Energy Mater.*, 2019, **9**, 8.
- W. Li, S. Albrecht, L. Yang, S. Roland, J. R. Tumbleston, T. McAfee, L. Yan, M. A. Kelly, H. Ade, D. Neher and W. You, *J. Am. Chem. Soc.*, 2014, **136**, 15566.
- B. Kan, H. Feng, H. Yao, M. Chang, X. Wan, C. Li, J. Hou and Y. Chen, *Sci. China: Chem.*, 2018, **61**, 1307.
- C. M. Proctor, J. A. Love and T.-Q. Nguyen, *Adv. Mater.*, 2014, **26**, 5957.

- 53 P. W. M. Blom, V. D. Mihailetschi, L. J. A. Koster and D. E. Markov, *Adv. Mater.*, 2007, **19**, 1551.
- 54 J. Gao, J. Wang, Q. An, X. Ma, Z. Hu, C. Xu, X. Zhang and F. Zhang, *Sci. China: Chem.*, 2020, **63**, 83.
- 55 J. Gao, W. Gao, X. Ma, Z. Hu, C. Xu, X. Wang, Q. An, C. Yang, X. Zhang and F. Zhang, *Energy Environ. Sci.*, 2020, **13**, 958.
- 56 C. M. Proctor, M. Kuik and T. Q. Nguyen, *Prog. Polym. Sci.*, 2013, **38**, 1941.
- 57 S. R. Cowan, A. Roy and A. J. Heeger, *Phys. Rev. B: Condens. Matter Mater. Phys.*, 2010, **82**, 245207.
- 58 L. J. A. Koster, V. D. Mihailetschi, R. Ramaker and P. W. M. Blom, *Appl. Phys. Lett.*, 2005, **86**, 123509.
- 59 P. N. Murgatroyd, *J. Phys. D: Appl. Phys.*, 1970, **3**, 151.
- 60 Y. Huang, E. J. Kramer, A. J. Heeger and G. C. Bazan, *Chem. Rev.*, 2014, **114**, 7006.
- 61 F. Zhao, C. Wang and X. Zhan, *Adv. Energy Mater.*, 2018, **8**, 1703147.
- 62 Y. Liu, X. Wan, B. Yin, J. Zhou, G. Long, S. Yin and Y. Chen, *J. Mater. Chem.*, 2010, **20**, 2464.
- 63 P. Müller-Buschbaum, *Adv. Mater.*, 2014, **26**, 7692.
- 64 J. Rivnay, S. C. B. Mannsfeld, C. E. Miller, A. Salleo and M. F. Toney, *Chem. Rev.*, 2012, **112**, 5488.
- 65 F. Liu, Y. Gu, X. Shen, S. Ferdous, H. Wang and T. P. Russell, *Prog. Polym. Sci.*, 2013, **38**, 1990.